

NEAR-TIP ANALYSIS OF CRACK PROPAGATION IN CEMENTITIOUS COMPOSITES

Eduardo B. Pereira⁽¹⁾, **Gregor Fischer**⁽²⁾ and **Joaquim A. O. Barros**⁽¹⁾

(1) Department of Civil Engineering, University of Minho, Portugal

(2) Department of Civil Engineering, Technical University of Denmark, Denmark

Abstract

The fracture process zone encloses relevant mechanisms which explain the quasi-brittle behavior of cementitious composites. It is an important concept in non-linear fracture mechanics and in the simulation of cracking processes. The use of fibers as reinforcement may alter the crack initiation and propagation processes. A better understanding of the micro-cracking mechanisms taking place at the level of the fracture process zone is therefore relevant for an optimized design of these materials, as well as for the simulation of their mechanical behavior. In this study, the use of an image analysis procedure to capture the crack initiation and propagation process in concrete and other cementitious composites is described. It utilizes high resolution digital images of the surface of the specimens while undergoing the cracking process to determine the displacement fields. The formed cracks are observed at a relatively small scale, allowing the investigation and analysis of propagating cracks near the crack tip in specimens of concrete and other cementitious composites.

1. INTRODUCTION

The transition zone between the fully developed crack and the intact bulk material ahead of the crack tip in propagating cracks encloses relevant mechanisms that determine the quasi-brittle behavior of cementitious composites and concrete. The moderate tensile hardening prior to the attainment of the ultimate tensile capacity and the subsequent rapid tensile softening that characterize the quasi-brittle behavior of concrete are explained by diffuse micro-cracking area forming ahead of the crack tip known as the fracture process zone [1,2,3]. The great attention that the scientific community devotes to the fracture process zone derives from its importance in non-linear fracture mechanics and in the simulation of cracking processes in cementitious composites. When fibers are used to restrain crack propagation, one immediate outcome are additional closing stresses that develop in the region of the macro-crack forming behind the propagating crack tip. However, the presence of the fibers may also have an effect in the region of the fracture process zone ahead of the crack tip, and therefore it may affect the mechanics of crack initiation and propagation. A better understanding of the micro-cracking mechanisms taking place at the level of the fracture process zone is therefore relevant for an optimal design of fiber reinforced cementitious composites (FRCC).

The research described in the literature towards a better understanding of the fracture process zone led to the development of special techniques of analysis of cracking. The very

fine cracks to be detected require high resolution equipments [4,5]. In addition, most of the intrusive characterization techniques used in other materials potentially induce preliminary cracks in concrete, either due to direct mechanical action, induced drying, or the alteration of other physical variables important for the delicate balance of the microstructure of concrete. Many different techniques have been especially developed for the analysis of the fracture process zone and cracking in concrete and other cement based materials. Radiography (x-rays, neutrons, or others), impregnation, acoustic emission, ultrasound, laser holography and interferometry represent some of the techniques that have successfully revealed quantitative information about the fracture process zone [5,6,7,8,9,10]. Although most of the macroscopic features of cracking processes in concrete are well understood, the micro-mechanisms of cracking and the essence of the fracture process zone still preserve some uncertainties. More qualitative and quantitative information about the fracture process zone is still required, as it can help improve the design of cement based materials and in particular the design of more efficient fiber reinforced cementitious composites.

Recent developments in digital photography technology have reached significant improvements in the quality of digital acquisition of images for scientific research. The new charged couple devices (CCD) of high resolution and quality allow the image-based documentation of cracking processes at small scales. In particular, the digital image correlation technique has been developed to obtain full field surface displacements and strains of objects under load, based on the comparison of two digitized images of the surface of an object before and after deformation [11]. Examples of applications of digital image correlation exist for the examination of deformations of distinct materials at different scales [12,13,14,15]. The method is not limited by an intrinsic length scale, which makes it very attractive for use over multiple length scales. The accuracy of the correlation between recorded images depends upon the quality of the image speckle pattern (including light conditions) and the resolution of the imaging system [16]. These factors make this technique appropriate for the observation of the displacements at the surface of concrete and other cementitious composites specimens with high resolution and detail.

2. EXPERIMENTAL PROGRAM

The testing procedure consisted of applying a tensile load to a single-edge notched specimen at a constant displacement rate of 5 $\mu\text{m/s}$, inducing the formation of a single crack and its subsequent propagation in a controlled manner. The specimen shape adopted resembles the one used for the evaluation of the crack growth behavior in metals [17], the so-called Compact Tension (CT) specimen. The unobstructed access to the surface where the crack progression becomes visible is the most relevant requirement of the present experimental procedure. With the purpose of maximizing the stress intensity at the tip of the notch, the notch thickness was minimized to 0.5 mm using a diamond cutting disc. The thickness of the specimen was also minimized (12 mm), promoting the plain stress state. The geometry and dimensions adopted for the specimens are presented in Figure 1. Two rods with a diameter of 22 mm were used to apply the load to the specimens, providing free rotation (Figure 2).

Four specimens with different compositions were tested: cement paste, mortar, concrete and FRCC. The composition of the cement paste consisted of cement and water only. The concrete composition consisted of the addition of aggregates with a maximum size of 4 mm to

the cement and water paste. The composition of the mortar and the FRCC consisted of cement, fly ash, fine sand (0.170 mm) water and admixtures, and Polyvinyl Alcohol (PVA) fibers as reinforcement in the case of the FRCC.

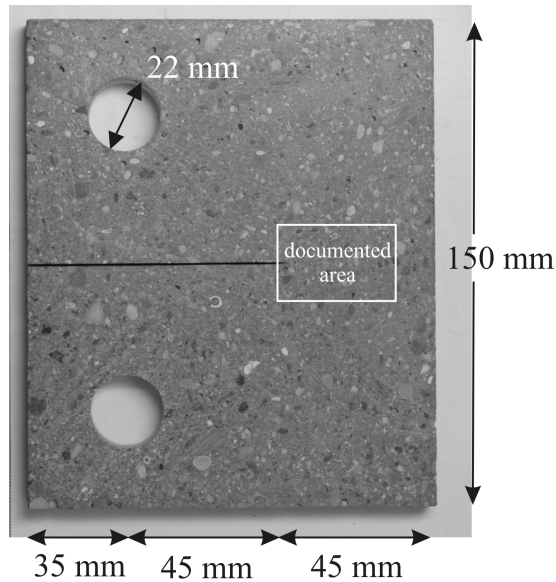


Figure 1. Specimen geometry.

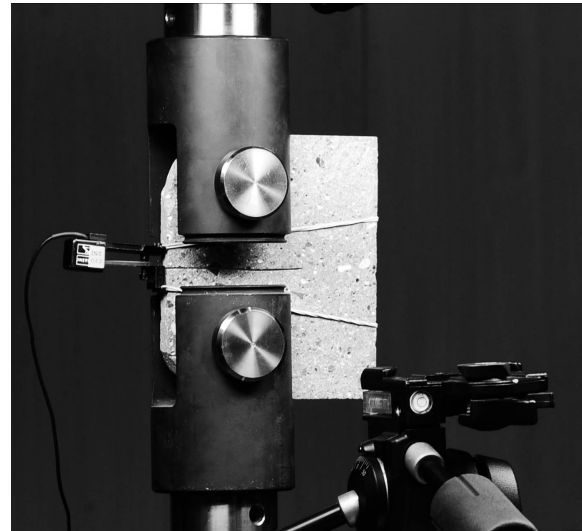


Figure 2. CT test setup.

The formation and propagation of the crack was traced on the surface of the specimens using a high resolution digital camera, positioned 90 mm away from the specimen. The 60 mm focal length lens allowed the observation of a 24 mm by 36 mm area of the surface of the specimen (see Figure 1). Images with resolution of 24 megapixel were captured during testing with time intervals of one second. These images were subsequently used for the continuous interpolation of the strain fields at the inspected surface of the specimen.

Sufficient randomness and high contrast of the stochastic patterns captured from the surface of the specimen are important for the effective analysis of the captured images [16]. In the present study, the natural features observed at the surface of the specimens were found to be sufficient for a satisfactory image correlation. Each facet was composed of 15×15 pixels. Each pixel covered an approximate area of $6 \times 6 \mu\text{m}^2$. The total area of $36 \times 24 \text{ mm}^2$ was modeled by a facet mesh overlay composed of approximately 400×260 facets.

3. RESULTS AND DISCUSSION

The results obtained in terms of load – crack mouth opening displacement (CMOD) during testing are presented in Figure 3. The CMOD was measured using a clip gage, positioned at the edge of the notch (Figure 2). The results are presented for CMOD values up to 1.6 mm.

In general, the load-CMOD curves obtained for the three non-reinforced cementitious matrices present a similar quasi-brittle behavior, with the cement paste reaching the lowest tensile load (86 N) and the concrete the highest (192 N). The post-peak softening branch in the concrete specimen showed a more gradual load decay compared to the other unreinforced cementitious matrices. The quantity and size of aggregates used in each matrix apparently

affected the fracture process, leading more and bigger aggregates to less sudden energy releases and abrupt load drops during softening. The PVA fibers in the FRCC specimen were responsible for a pronounced tensile hardening stage after the first peak load (initial peak). The maximum tensile load reached was 304 N (global peak) at a CMOD of 1.46 mm.

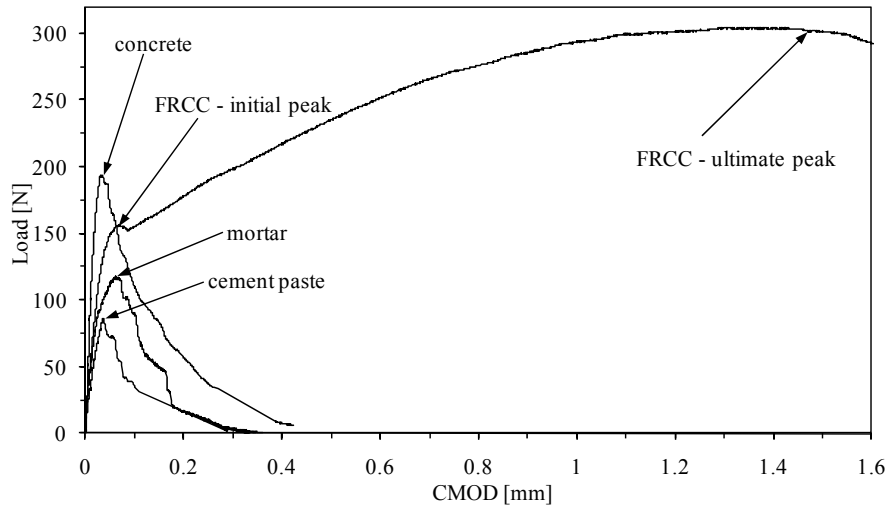


Figure 3. Load – CMOD curves measured during testing. The peak loads are identified with an arrow for all specimens.

3.1 Crack initiation and propagation

In Table 1, the results obtained with the image-based monitoring system are shown. The maximum principal strains derived from the interpolated displacement fields at the facets overlay are presented. The color gradients evolve from dark grey (zero strain) to white (maximum strain of 5%). These strain values refer to the displacement gradients derived at the facets overlay, according to the principles of linear elasticity [11].

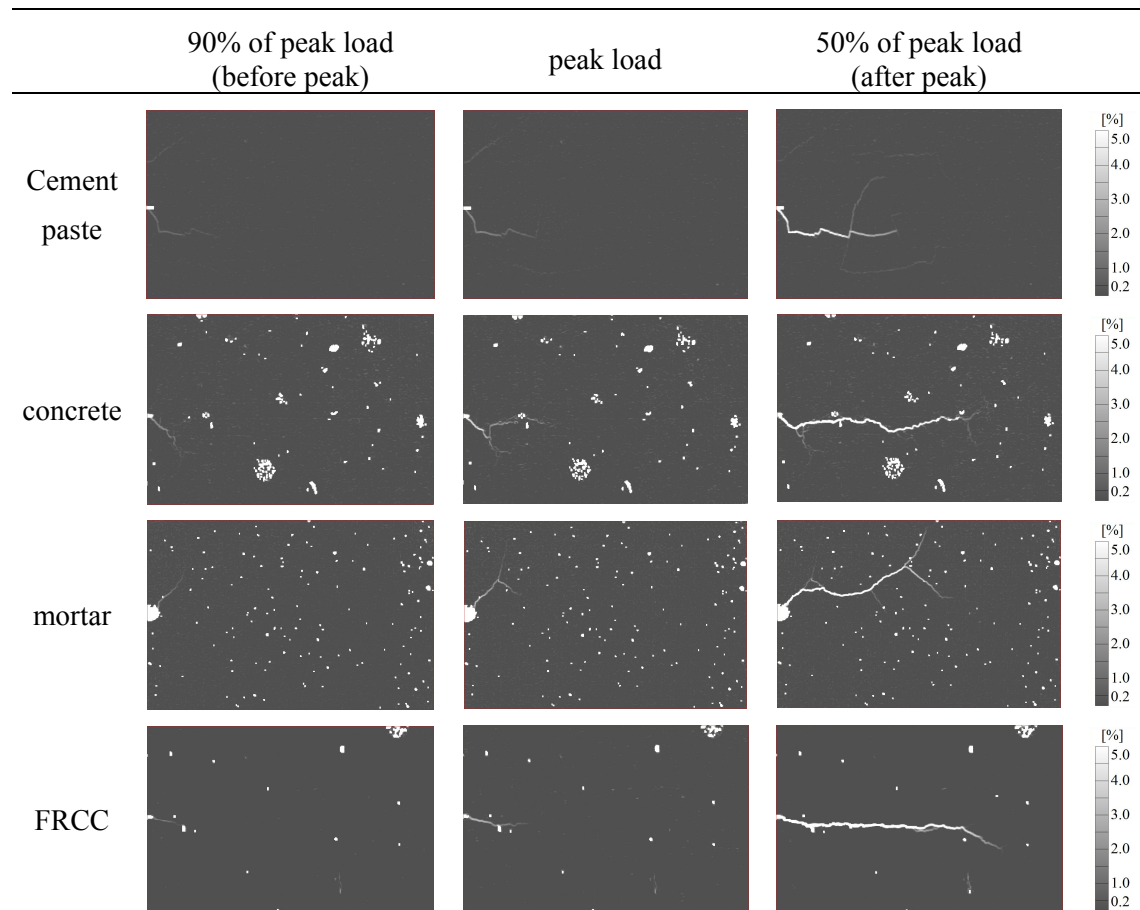
To illustrate the obtained results, three representative stages were selected: before the peak load was reached (90% of the peak value), when the peak load was reached and after the peak load (50% of the peak value). In the case of the FRCC specimen, the peak load refers to the first peak load.

The images in Table 1 show that the technique reveals high sensitivity for detecting very small cracks. When 90% of the peak load is reached the opening at the tip of the notch is 4 μm for the cement paste specimen, 4 μm for the mortar, 5 μm for the concrete and 4 mm for the FRCC. For all specimens the measured deformations reveal the early initiation of the cracks at the tip of the notch well before the peak load was reached.

The effect of crack branching is visible in all the specimens tested although they are assuming different detailed features. In the mortar specimen, the crack branches developed are fewer, longer and more discrete. In the concrete specimen the crack branching occurs more frequently and the branches of the main crack are less visible and more diffuse. A small area of diffuse micro-cracking ahead of the principal crack is visible in some stages as well. The increase in the number of aggregates and their size contributed to the increase of crack smearing. At the same time, the smaller and more frequent crack branches formed suggest

that the smearing of the crack tip contributes to the gradual dissipation of the energy associated with the fracture process. In the FRCC specimen, branching and crack smearing are less visible probably due to the contribution of the fibers to arresting the propagation of micro-cracks. Observing the results obtained with the cement paste specimen (Table 1), secondary cracks become visible right from the onset of the testing sequence. These secondary cracks were not connected to the principal crack initiating at the tip of the notch suggesting that these are probably shrinkage cracks that become active when the specimen is loaded. The crack path seems to be greatly influenced by these pre-existing shrinkage cracks. They may also explain the lower initial stiffness observed in the load-CMOD diagram of the cement specimen.

Table 1. Maximum principal strains in the facet overlay for three load levels: before peak load (90% of the peak load); when peak load is reached; after peak load (50% of the peak load).



3.2 Effect of fibers in the fracture process zone

The influence of fibers in the fracture processes and crack propagation was evaluated by investigating the crack profiles obtained in the mortar and the FRCC specimens. The morphology of the principal crack formed in the mortar specimen is depicted in Figure 4 at five distinct loading stages: before the first peak load when 90% of the load is reached (P-10%), when the peak load is reached (P), and after the peak load is reached for 90% of the peak load (P-10%), 80% of the peak load (P-20%) and 50% of the peak load (P-50%). The

crack profiles were obtained by computing the evolution of the distance difference between two points placed in opposite sides of the principal crack. Thirty of these virtual clip gages were placed evenly spaced (1 mm) along an initial portion of the macro-crack measuring 30 mm, starting from the tip of the notch.

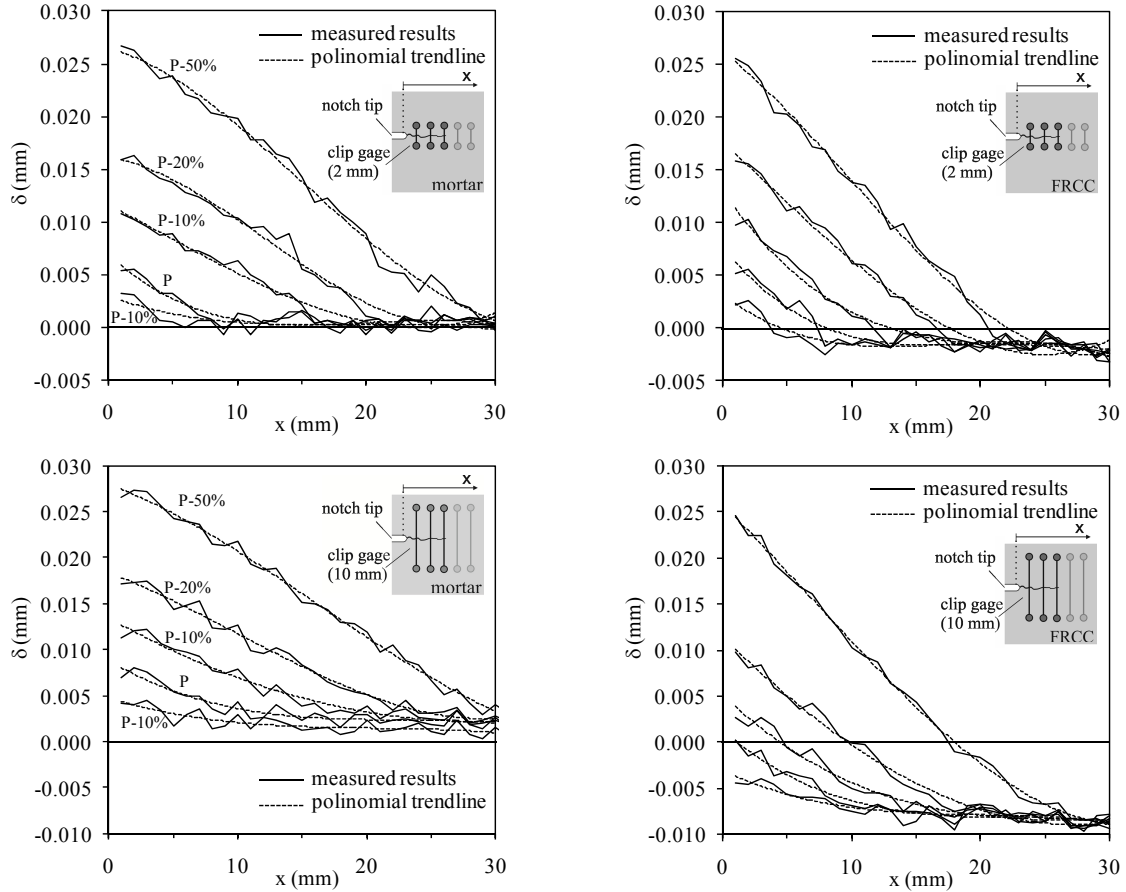


Figure 4. Crack profiles obtained for different loading stages of the mortar and the FRCC specimens using two virtual clip gage sizes (2 mm and 10 mm).

In general, the results presented in Figure 4 reveal that the displacements measured in the virtual clip gages follow approximately the shape of a third order polynomial trend line. Significant differences between the general shapes in the mortar and in the FRCC specimens can although be observed. In the case of the mortar specimen, when using the 2 mm virtual clip gages the open crack portion of the displacement profiles seems to gradually change from a single curvature shape to double curvature. When these crack profiles are compared with the ones obtained with the FRCC specimen, the gradual transition from a single to a double curvature shape is no longer observed. For comparison, the five stages selected for the FRCC were the ones in which the crack opening at the tip of the notch ($x = 0$) was approximately identical to the respective ones observed in the five load stages selected for the mortar specimen, while using the 2 mm virtual clip gages. This comparison allows also the observation that cracks with the same opening at the tip of the notch ($x = 0$) show a much smaller length in the case of the FRCC than in the mortar specimens. Additionally, in the case

of the FRCC specimen, the relative displacements in the region ahead of the tip of the crack are negative, which may result from the bridging stresses provided by the fibers in the region of the open crack. These additional compression strains/stresses in the region ahead of the crack tip affect the propagation of the crack by promoting the rapid transition from the undamaged bulk material to the fully open crack through a smaller length.

The use of the virtual clip gages with a length of 10 mm instead of the 2 mm aimed at helping to distinguish the area around the crack which was predominantly affected by the crack propagation. Figure 4 shows that the differences observed previously regarding the curvature of the displacement profile in the region of the open cracks are similar but less evident. The compression strains observed ahead of the crack tip become more pronounced in the case of FRCC contrarily to the mortar specimen where small tensile strains are observed through the whole monitored length even at the early stages of the cracking process. This suggests that the contribution of the fibers in the case of the FRCC results in the overall increase of the ambient compression stresses surrounding the fracture process zone, which in turn contribute to the reduction of the crack length for the same CMOD and the reduction of the size of the transition region between the open crack and the intact bulk material. Due to the reduced post-peak residual tensile stresses in the mortar, the ambient stresses surrounding the crack tip region are tensile and develop along the full monitored length even at the early crack stages. As a consequence, the stabilization of the cracking processes and crack propagation resulting from the adoption of the fibers was not only a direct consequence of the fiber contribution for crack bridging but also a result of the alteration of the stress and strain fields surrounding the crack tip. Not only the shape but also the length of the transition zone between the fully open crack and the intact bulk material were changed or affected by the presence of the fibers.

4. CONCLUSIONS

The analysis of propagating cracks in cementitious composites with an image-based monitoring technique presented in this study allowed the interpretation of the relevant micro-mechanical events taking place during the initiation and propagation of the cracks, as well as the investigation of their relation with the observed mechanical behaviors. The influence of shrinkage induced pre-existing cracks on the path of the principal crack was revealed by the images of the cement paste specimen. The pre-existing cracks may also explain the smaller initial stiffness observed in the cement paste specimen. Similarly, the presence of different quantities and sizes of aggregates influenced the morphology of the propagating cracks especially near the crack tip. In the cementitious composites containing more and larger aggregates, the observed cracks developed shorter and more smeared crack branches, sometimes even a small, diffusely cracked area ahead of the crack tip was observed. In the FRCC specimen the crack branches were less visible, suggesting that the fibers have contributed effectively to the micro-cracking arrestment.

The investigation of the displacement profiles along the cracks formed in the mortar and in the FRCC specimens led to the conclusion that the shape of the crack was altered by the use of fibers as reinforcement. Also the crack lengths observed at different loading stages at the same crack tip opening displacements (CTOD) were reduced in the case of the FRCC. The presence of the fibers in the FRCC was shown to affect the mechanical behaviour of the composite not only by contributing to the crack bridging in the region of the open crack but

also by changing the ambient strains surrounding the crack tip region and in particular altering the size and boundary conditions of the fracture process zone.

ACKNOWLEDGMENTS

The authors thank the Portuguese National Science Foundation for the financial support, through grant SFRH / BD / 36515 / 2007, funded by POPH - QREN, the Social European Fund and the MCTES, and DTU-Byg for their support of the work as part of this project.

REFERENCES

- [1] Karihaloo B.L., Carpinteri A., Elices M., 'Fracture mechanics of cement mortar and plain concrete' *Adv. Cem. Based Mater.* **1** (1993) 92-105.
- [2] Landis E.N., Shah S.P., 'The influence of micro-cracking on the mechanical behavior of cement based materials', *Adv. Cem. Based Mater.* **2** (1995) 105-118.
- [3] Wittmann F.H., Xiaozhi H., 'Fracture process zone in cementitious materials' *Int. J. Fracture* **51** (1991) 3-18.
- [4] Hornain H., Marchand J., Ammouche A., Commène J.P., Moranville M., 'Microscopic observation of cracks in concrete – a new sample preparation technique using dye impregnation', *Cement Concrete Res.* **26**(4) (1996) 573-583.
- [5] Otsuka K., Date H., 'Fracture process zone in concrete tension specimen', *Eng. Fract. Mech.* **65** (2000) 111-131.
- [6] He S., Feng Z., Rowlands R.E., 'Fracture Process Zone Analysis of Concrete Using Moiré Interferometry', *Exp. Mech.* **37**(3) (1995) 367-373.
- [7] Knab L.I., Walker H.N., Clifton J.R., Fuller Jr. E.R., 'Fluorescent thin sections to observe the fracture zone in mortar', *Cement Concrete Res.* **14** (1984) 339-344.
- [8] Landis E.N., Zhang T., Nagy E.N., Nagy G., Franklin W.R., 'Cracking, damage and fracture in four dimensions', *Mater. Struct.* **40** (2007) 357-364.
- [9] Regnault P.H., Brühwiler E., 'Holographic interferometry for the determination of fracture process zone in concrete', *Eng. Fract. Mech.* **35** (1990) 29-38.
- [10] Shah S.P., 'Experimental methods for determining fracture process zone and fracture parameters', *Eng. Fract. Mech.* **35** (1990) 3-14.
- [11] Chu T.C., Ranson W.F., Sutton M.A., Peters W.H., 'Applications of digital-image-correlation techniques to experimental mechanics', *Exp. Mech.* **25**(3) (1985) 232-244.
- [12] Abanto-Bueno J., Lambros J., 'Experimental determination of cohesive failure properties of a photodegradable copolymer', *Exp. Mech.* **45**(2) (2005) 144-152.
- [13] Corr D., Accardi M., Graham-Brady L., Shah S., 'Digital image correlation analysis of interfacial debonding properties and fracture behavior in concrete', *Eng. Fract. Mech.* **74** (2007) 109-121.
- [14] Savic V., Hector Jr L.G., Fekete J.R., 'Digital image correlation study of plastic deformation and fracture in fully martensitic steels', *Exp. Mech.* **50** (2010) 99-110.
- [15] Yoneyama S., Morimoto Y., Takashi M., 'Automatic evaluation of mixed-mode stress intensity factors utilizing digital image correlation', *Strain* **42** (2006) 21-29.
- [16] Berfield T.A., Patel J.K., Shimmin R.G., Braun P.V., Lambros J., Sottos N.R., 'Micro- and nanoscale deformation measurement of surface and internal planes via digital image correlation', *Exp. Mech.* **47** (2007) 51-62.
- [17] ASTM-E647, 'Standard test method for measurement of fatigue crack growth rates', (*ASTM Standards* Vol. 03.01, US, 2005).